Scientific
Research
Publishing

TEC Variability during Fluctuating Events at Koudougou Station during Solar Cycle 24

Tinlé Pahima, Doua Allain Gnabahou*, Sibri Alphonse Sandwidi, Frédéric Ouattara

Research Laboratory in Energetics and Space Weather (LAREME), University Norbert Zongo (UNZ), Koudougou, Burkina Faso
Email: *gnabahou@yahoo.fr

Abstract

This paper deals with TEC variability during fluctuating geomagnetic events (FE) during solar cycle 24 at Koudougou station (lat: 12˚15'N; Geo long: −2˚20'E). The study was done by comparing TEC variations during FE days with those of quiet days (QA). Comparison was made taking into account solar phases' and seasons' influences. FE's and QA's TEC curves are characterized by dome profiles. All graphs show two troughs, one in the morning (0500 LT) and the second in the evening (around 2000 LT) and a peak around 1400 LT during all solar phases and winter months and around 1500 LT for the remaining seasons. Both troughs are caused by the decrease of the photo ionization and an increase of the recombination phenomena, as well for FE as for QA periods. FE cause positive storms during all solar phases as well as during seasons and some negative storms during spring and summer months and minimum and maximum solar phases.

Keywords

Total Electronic Content, Fluctuating Events, Solar Cycles, Photoionization, Recombination, Positive Storms, Negative Storms

1. Introduction

Ionosphere is Earth's atmosphere' ionized layer where optical effects occur. The effect of ionospheric refraction on satellite signals depends on the total electron content (TEC). TEC is free electrons number in the ionized plasma contained in an imaginary tube of 1 m² cross-section, the ends of which are bounded by the orbiting satellite and the ground receiver [1]. The photoionization and recombination processes characterize the electronic production phenomena. The for-

mer is the process of transformation of atoms and molecules into ions under solar radiation impact. It depends on the incident ultraviolet radiation intensity which is itself a function of local time, altitude, season and solar activity. Recombination is the reverse process consisting of the recombination of positive ions and free electrons to form atoms and molecules.

According to Boutiouta and Belbachir [2], TEC's evolution is strongly correlated with solar activity. This is the signature of solar flares which evolve with sunspot cycle [3]. TEC's variations are analyzed to understand ionosphere's responses to space weather phenomena. A number of studies suggest ionospheric disturbances caused by external (e.g., magnetospheric storms) and internal (e.g., gravitational waves) factors as TEC's variations main source [4] [5] [6]. Results of these works revealed several explanatory phenomena for TEC variation. These include 1) equatorial plasma bubbles (EPB), 2) the equatorial electrojet (EEJ), 3) the equatorward circulation of the thermospheric neutral wind (TNWC), 4) magnetic storms, 5) the phenomenon of electric field enhancement prior to reversal (PRE).

Plasma bubbles are plasma irregularities that originate in the equatorial (low-latitude) ionosphere under Rayleigh-Taylor instability (RTI) conditions and they can propagate to higher latitudes [7] [8]. The EEJ is an intense eastward flowing current in the dynamo region (E layer) through the Equatorial Ionization Anomaly (EIA) zone in a narrow band ±3˚ on either side of the magnetic equator [9] [10] [11]. Storms resulting from magnetic disturbances in the ionosphere under intense solar activities influence cause the ionospheric electron density to increase (positive storm) or decrease (negative storm) [12] [13] [14] [15]. The PRE is a strong eastward enhancement of diurnal electric field near magnetic equator shortly after sunset (1700 - 1900 TL) [16].

Several studies have already been conducted on TEC variations during disturbed geomagnetic activities. It has been found in general that TEC variations follow solar activity trend [17]-[22]. In other words, TEC variations increase with solar activity intensity. Therefore, deviations between disturbed and quiet activities profiles will be larger at solar maximum phase than at minimum. Picanço *et al.* [8] observed the same result by highlighting that EPB-related TEC perturbations tend to be higher (or lower respectively) when solar activity is high (or low respectively). Zoundi *et al.* [21] also obtained a correlation between TEC variations and solar activity by analyzing Niamey station (lat.: 13˚28'N; long: 2˚10'E) TEC variability during fluctuating activities (FA).

This paper aims to analyze TEC variations during solar cycle 24 at Koudougou station (Geo. lat 12˚15'N; Geo log: −2˚20'E). The novelty of this study is that it is the first to be carried out at Koudougou station using the new classification (NC) and considering the whole solar cycle 24. It consists in determining fluctuating winds impact on TEC variations by comparing those of fluctuating days to those of quiet days. Section 2 is devoted to Materials and methods. Section 3 presents the Results and discussions and section 4 is devoted to conclusion.

2. Materials & Methods

2.1. Data

TEC data used are from Koudougou GPS station. The receiver was provided by the Ecole Nationale de Télécommunication of Bretagne (ENST Bretagne) as part of the International Heliophysical Year (IHY) project initiated by Europe-Africa Study and Research Group (GIRGEA). This receiver has been installed at University Norbert ZONGO since November 2008. TEC data recorded cover solar cycle 24, except for the years 2008; 2018 and 2019. The geomagnetic index data *aa* and the dates of Sudden Storm Commencement (SSC) were used [23] to elaborate the pixel diagram. This diagram represents geomagnetic index *aa* evolution as a function of solar activity for each Bartels rotation [24]. The mean sunspot number (*Rz*) annual was used for the division of the solar cycle 24 into phases.

The geomagnetic index *aa* is deduced from K-index measured at two mid-latitude antipodal stations. This index measures the amplitude of global geomagnetic activity during 3-hour intervals normalized to geomagnetic latitude ±50°. It was introduced by Mayaud [25] to monitor geomagnetic activity over the longest possible period. The daily average of the 8 tri-hourly values per day is noted *Aa*. An SSC corresponds to an abrupt change in the geomagnetic field followed by a geomagnetic storm that lasts less than an hour. The dates of SSCs and the values of the *aa* index since 1869 are available on the ISGI website (http://isgi.unistra.fr). *Rz* values are available on the OMNIWEB website: https://omniweb.gsfc.nasa.gov/form/dx1.html.

2.2. Geomagnetic Activities' Classification Methods

Legrand and Simon [26]; and Richardson *et al.* [27] [28] elaborated geomagnetic activities' first classification from pixel diagram. They classified geomagnetic activities into four classes: 1) quiet activities associated with slow solar winds (*V* < 450 km/s); 2) recurrent activities caused by fast solar winds from coronal holes (*V* > 450 km/s); 3) shock activities related to shock waves due to Coronal Mass Ejections (CMEs); and 4) fluctuating activities caused by fluctuations in the Sun's neutral blade. Ouattara and Amory-Mazaudier [29] continued, in the same dynamics, by improving this method.

This classification was further improved by Zerbo *et al.* [30], who pushed the limits of old classification (AC) by providing clarification of solar origin of about 20% of the geomagnetic storms in addition to the 60% explained by AC. In new classification (NC), days of quiet activity, associated with slow solar winds, correspond to days when *Aa* < 20 nT and disturbed activity to days when *Aa* ≥ 20 nT. Disturbed days include: 1) fluctuating activity days (AFs) or fluctuating events (FEs) caused by fluctuations in the Sun's neutral blade, 2) shock events (SEs) including shock activity (SA) and cloud shock activity (CSA), and 3) recurrent event days (REs) including classical recurrent activities of AC (RAs) and Corotating Moderate Activities (CMA) due to stable corotating neutral winds.

Geomagnetic activity days selection is done using the pixel diagram (**Figure 1**)

proposed by Simon and Legrand [31] and improved by Ouattara and Amory-Mazaudier [29] who organized it in columns and rows; then they defined a color code to identify different types of geomagnetic activities. A line in the diagram corresponds to a solar rotation (27 days). The SSC dates are indicated by circles surrounding the corresponding *aa* index value. The dates of the beginning days of Bartels cycle, the legend and the year are shown on the left, right and above the pixel diagram respectively. According to pixel diagram color code, different geomagnetic activities days are selected as follows:

1) Quiet activities (QA) corresponding to days with $Aa < 20$ nT which are represented by white and blue boxes;

2) Recurring events (RE) including:

a) classical recurrent activities (RA) of AC corresponding to days with $Aa \geq 40$ nT and spanning one or more Bartels rotations without SSC; these days are represented by orange, red, and/or dark red boxes on at least two successive days without SSC and on at least two solar rotations;

b) and CMA days corresponding to days with 20 nT $\leq Aa < 40$ nT and spanning one or more Bartels rotations without SSC; these days are represented by yellow or green boxes on at least two successive days without SSC and on at least two solar rotations

3) Shock events (SE) including:

a) Classical shock activities of AC (SA) corresponding to SSC days with $Aa \geq 40$ nT; these days are represented by a set of 1, 2, or 3 days represented by orange, red, and/or olive-red boxes with SSC in phase beginning and no recurrence of SSC during 1, 2, 3, or 4 Bartels rotations;

b) and CSA days corresponding to SSC days where 20 nT $\leq Aa < 40$ nT; these days are represented by a set of 1, 2, or 3 days represented by yellow and green boxes with SSC at phase beginning and no recurrence of SSC during 1, 2, 3, or 4 Bartels rotations

4) Fluctuating events (FE) which include all days not included in three previous classes.

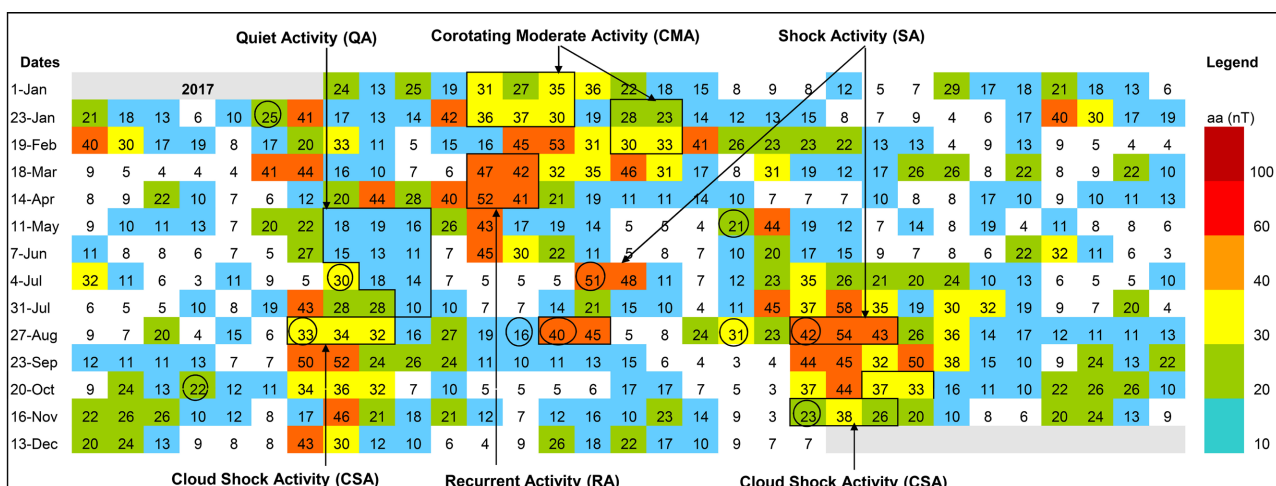

Figure 1. Pixel diagram showing the different geomagnetic activities according to the NC.

2.3. Solar Phases Determination Criteria

Solar cycle is divided into phases according to criteria proposed by Ouattara and Amory-Mazaudier [29]. These criteria related to the annual average of sunspots number Rz are defined as follows: 1) minimum phase: $Rz < 20$; 2) ascending phase: $20 \leq Rz \leq 100$ with Rz greater than that of previous year; 3) maximum phase: $Rz > 100$ noting that for weak solar cycles (with $Rzmax < 100$) the years of maximum phase correspond to those with an index $Rz > 0.8\ Rzmax$, and 4) decreasing phase: $100 \geq Rz \geq 20$ with Rz lower than that of the previous year.

However, since 2015, a new set of Rz values different from the one used by Ouattara and Amory Mazaudier [32] is available on the OMNIWEB website (https://omniweb.gsfc.nasa.gov/form/dx1.html). Considering the previous Rz values that are limited to 2014, cycle 24 is low because its peak that corresponds to the year 2014 is less than 100 ($Rz = 78.9$). Since the previous Rz values ($R_{Z\_previous}$) do not exist beyond the year 2014, equations 1 and 2 were used to find the approximate values of $R_{Z\_previous}$ equivalent to those of the Rz new values (R_{Z_new}) for the missing years of cycle 24 (2015 to 2018) in order to be able to use the criteria of Ouattara and Amory-Mazaudier [32]. **Table 1** summarizes solar cycle 24' previous, new and approximate Rz values.

$$\sigma_1 = \frac{R_{Zancien}}{R_{Znouveau}} \tag{1}$$

$$\sigma_2 = \frac{\sum_{2008}^{2014} \sigma_1}{7} \tag{2}$$

Equation (2) gives $\sigma_2 = 0.679709088$

$R_{Z\_approximate}$ is the approximate value of $R_{Z\_previous}$. It's estimated by the Equation (3).

$$R_{Z\_approximate} = R_{Znew} \times \sigma_2. \tag{3}$$

Table 2 shows results of solar cycle 24 cutting into phases.

Table 1. Previous, new and approximate annual average *Rz* values.

Years	2008	2009	2010	2011	2012	2013	2014	2015	2016	2017	2018
$R_{Z\ old}$	2.9	3.1	16.5	55.7	57.7	64.9	78.9				
$R_{Z\ new}$	4.2	4.8	24.9	80.8	84.5	94	113.3	69.8	39.8	7	3.6
$R_{Z\ app\_old}$								47.4	27.1	14.7	4.8

Table 2. Results of solar cycle 24 cutting into phases.

Phases	Corresponding years
Minimum	2008; 2009 and 2010
Ascending	2011 and 2012
Maximum	2013 et 2014
Descending	2015; 2016; 2017 and 2018

2.4. Seasons Determination Criteria

Several studies have demonstrated TEC variability seasonal dependence. Some have revealed the existence of semi-annual variations characterized by electron density peaks at equinoxes [33] [34] [35] [36]; while others revealed a winter anomaly existence characterized by peaks in winter versus summer [33] [34] [35] [36]. Seasons are defined as follow: winter (December, January, February), spring (March, April, May), summer (June, July, August), and fall (September, October, November).

2.5. Data Analysis Methods

The error bars placed on TEC profiles of the QA, for the qualitative analysis of FE compared to QA, are obtained by $\delta = \sqrt{V}$ where V is the variance given by Equation (4).

$$V = \frac{\sum_{i=1}^{N}\left(TEC_i - \overline{TEC}\right)^2}{N} \tag{4}$$

With TEC_i the hourly values of TEC; $\overline{TEC}$ the average hourly value of daily hourly values and N the total number of days depending on solar phase or season considered.

Based on the definition of storm strength as defined by Vijaya Lekshmi *et al.* [37], the relative deviation of TEC (δTEC), allowing the type and the intensity of the observed storm to be assessed, is defined by the Equation (5):

$$\delta TEC = \frac{\overline{TEC_F} - \overline{TEC_q}}{\overline{TEC_q}} \times 100 \tag{5}$$

where $\overline{TEC_F}$ and $\overline{TEC_q}$ denote the average hourly values of TEC in fluctuating and quiet periods respectively.

The storm is qualified as positive, respectively negative, when $\delta TEC > 0$, respectively $\delta TEC < 0$.

For δTEC values between $\mp 20\%$ the storm is considered to be weak or moderate; otherwise, it is called an intense storm.

The solar cycle 24's (January 1, 2008 to December 31, 2018) FE and QA days were counted in order to analyze their occurrences. The study included 2939 QA days and 697 FE days. The occurrence rates are obtained using the formula in Equation (6).

$$\%Occ = \frac{N_A}{N_T} \times 100$$

where N_A is the number of QA or FE days per solar phase or season considered and N_T is the total number of days per solar phase or or by the considered season.

3. Results and Discussions

3.1. Results

3.1.1. Fluctuating Events' Occurrence Per Season and Per Solar Phase
Figure 2 shows the fluctuating events (FE) and quiet activities (QA) occurrences

by solar phase (panel "a") and by season (panel "b"). QA are more predominant than FE during minimum and maximum solar phases. The predominance of QA at solar maximum could be explained by the fact that solar cycle 24 is a weak solar cycle (its maximum Rz value (78.9) is smaller than 100) [32]. FE appear more at the increasing and descending phases with respective occurrence rates of 21.66% and 47.20%. QA predominate over FE during all seasons except spring when FE appear very considerably with an occurrence rate of 28.69%.

3.1.2. Fluctuating Events (FE) Effects on TEC Diurnal Variations by Solar Phase

Figure 3 shows TEC diurnal variations profiles and the relative deviation δTEC between FE and QA. Solid curves and dashed curves relate respectively to QA and FE. These graphs are used to study FE impact on TEC variations by solar phase at Koudougou station. Panels "a", "b", "c" and "d " are assigned respectively to minimum, increasing, maximum and decreasing phases. In panels "a", "b", "c" and "d" TEC's profiles show the same trend. It's observed a slight decrease in TEC (from 0000 LT to 0500 LT), an increase (from 0500 LT to 1400 LT), and a further decrease (from 1400 LT to 2300 LT).

At minimum phase, FE and QA's curves show some differences. Qualitatively the error bars highlight that the difference is considerable from 1100 to 2300 LT. Both graphs present peaks around 1400 LT with values of 32.92 TECU and 29.32 TECU respectively. δTEC's graph indicate that FE cause positive storms during day time, except at 0300 LT, 0400 LT and 0700 LT. These storms are intense (ie $\delta TEC > 20\%$) throughout the night (2000 - 2300 LT) with a peak observed around 2200 LT ($\delta TEC \sim 32.25\%$).

In increasing phase, both graphs overlap almost all time. δTEC values show that storms remain positive during all day time. The FE's days are predominant over QA's days as observed by Ouattara *et al.* (2017). This could explain the positive storms observed during all the day, even though they are moderate ($\delta TEC < 20\%$).

At maximum, both graphs keep the same morphology. Error bars in QA's curve highlight that the deviations are not really considerable. δTEC's values

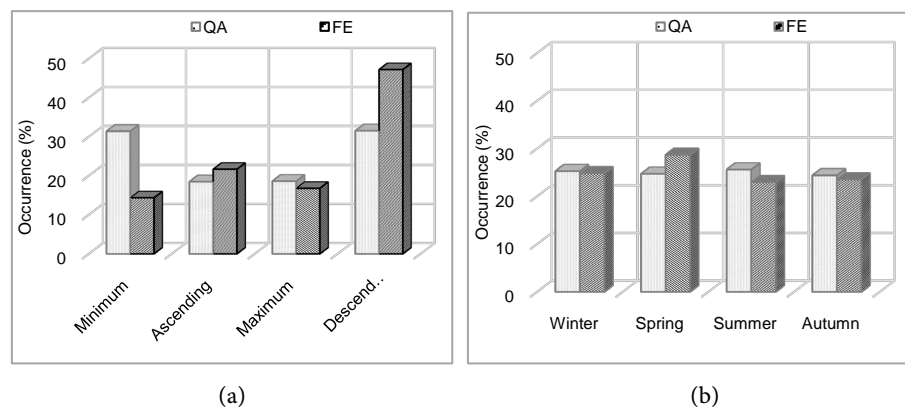| | (a) | | (b) |

Figure 2. Fluctuating events occurrence variability by solar phase (a) and per season (b).
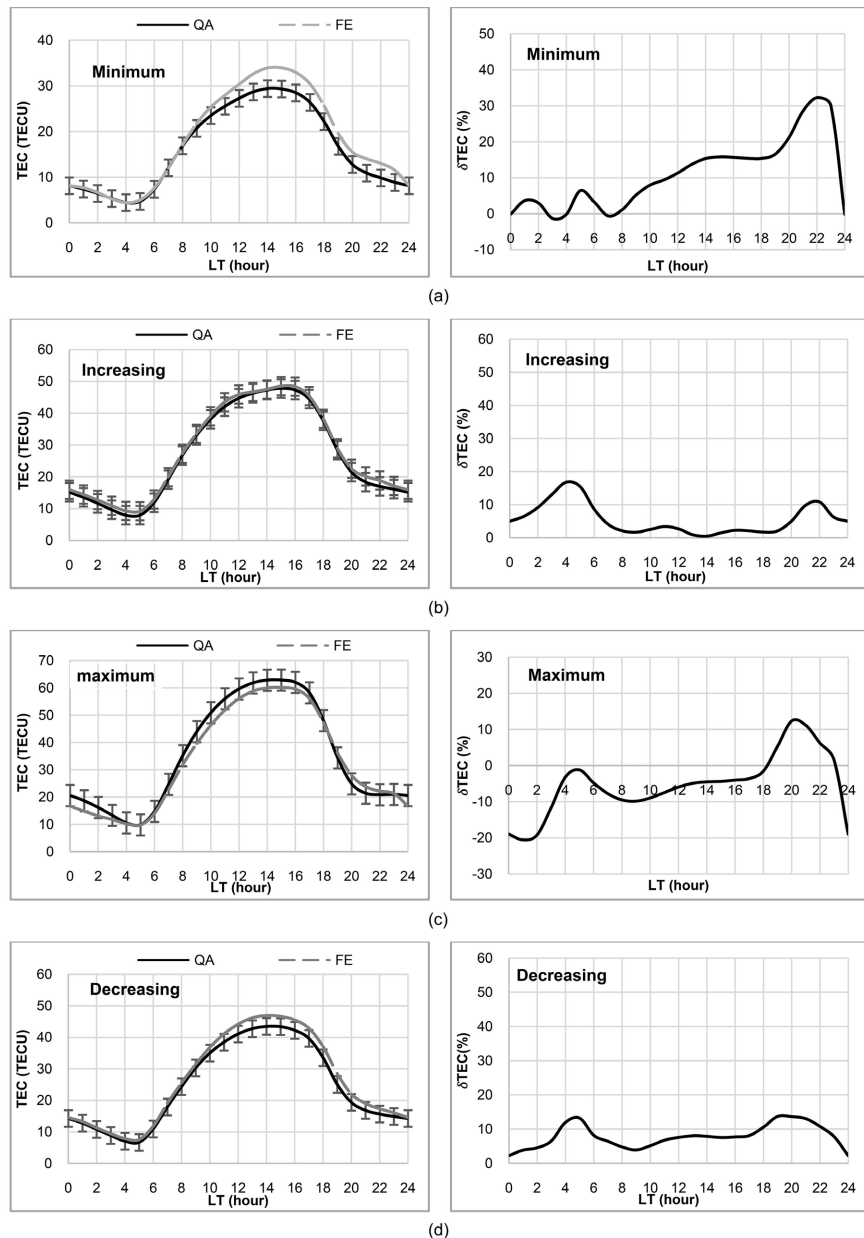
Figure 3. Solar phases' influence on TEC diurnal variations during fluctuating events (FE).

show that storms are negative during all the day time, except from 1900 LT to 2300 LT. Storms remain moderate during because δTEC values are between $\mp 20\%$, except around 0100 LT. Peaks of moderate positive storms are observed after sunset (1900 - 2200 LT).

At decreasing phase, both curves present a similar morphology with peaks of 46.89 TECU and 43.47 TECU observed around 1400 LT for fluctuating and quiet events respectively. δTEC's values highlight the presence of positive storms during all the day time. Error bars show that the difference is not very significant. The storms are weak at all times because $\delta TEC < 10\%$ except from 0400 LT to 0500 LT and from 1800 LT to 2200 LT when $10\% < \delta TEC < 20\%$.

3.1.3. Fluctuating Events (FE) Effects on TEC Diurnal Variations Per Season

Figure 4 shows TEC diurnal variations profiles and the relative deviation δTEC between FE and QA. Solid curves and dashed curves relate respectively to QA and FE. These graphs are used to study FE impact on TEC variations by season at Koudougou station. Panels "a", "b", "c" and "d" are assigned respectively to spring, summer, autumn and winter. In the panels, TEC's profiles show the same trend. A sharp decrease of the TEC is observed (from 0000 LT to 0500 LT), followed by an increase trend (from 0500 LT to 1400 LT) and a further decrease (from 1400 LT to 2300 LT).
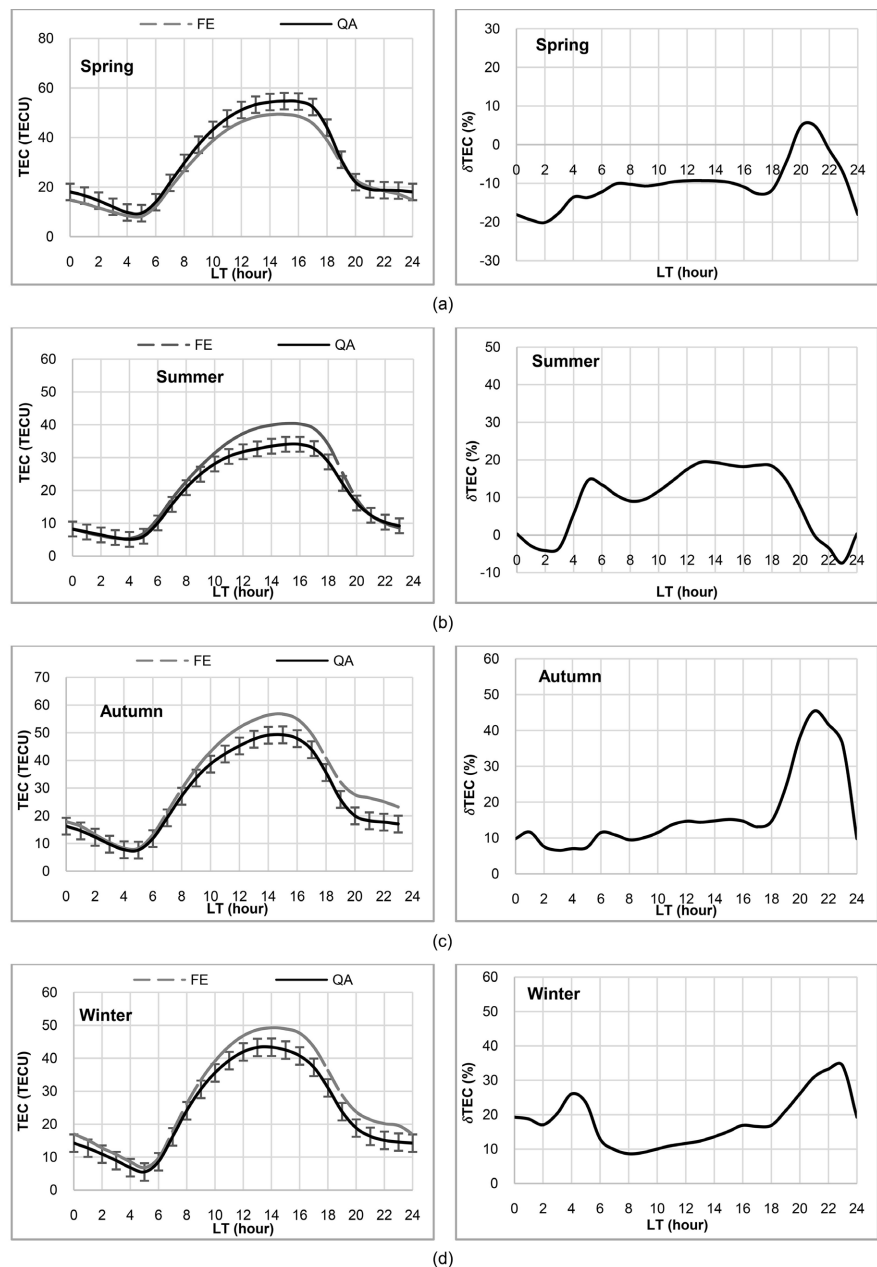

Figure 4. Seasons' influence on TEC diurnal variations during fluctuating events (FE).

During all seasons, FE's and QA's curves show a trough generally around 0500 LT. This trough and also the trend of TEC decreasing during night can be related to the recombination process. Recombination phenomenon is a process responsible of ionospheric electron drop by the recombine of positive ions and free electrons to produce atoms and neutral molecules. Therefore, the trough observed at dawn reflects a decrease in photoionization at night and an increase in recombination phenomena, both for FE and QA.

Peaks are generally observed around 1500 LT in spring (54.69 TECU for QA and 49.36 for FE), in summer (40.40 TECU for FE and 34.05 TECU for QA), in autumn (56.73 TECU for FE and 49.25 TECU for QA). In winter, peaks are observed with values of 49.25 TECU (for FE) and 43.35 TECU (for QA). FE's curves are above those of QA during all hours of the day for autumn and winter seasons. Indeed, δTEC's values for both seasons show that storms remain generally positive and moderate during all the day time. Storms are intense ($\delta TEC >$ 20%) from 1900 LT to 2300 LT (for both seasons) and also from 0300 LT to 0500 LT for winter.

For spring season, storms remain negative all the day time, except from 2000 LT to 2100 LT. Concerning summer, storms are generally positive and moderate during day time, except from 0000 LT to 0300 LT where they are negative and moderate.

3.2. Discussions

From analysis of impact of FEs on the diurnal variations of the TEC, it appears that:

1) FEs generate positive storms during all the day time and during all phases, except at maximum phase. Moderate negative storms are observed at solar maximum (from 0000 LT to 1800 LT) and weak negative storms at solar minimum around 0300 and 0700 LT. Concerning seasons, positive storms are observed during all hours in winter and autumn. For spring, negative storms are observed during all the day time, except from 2000 to 2100 LT. But for summer, positive storms are observed from all the day, except from 0000 LT to 0300 LT and from 2100 LT to 2300 LT.

2) Troughs are observed at 0500 LT and 2000 LT during all solar phases and seasons. Patel *et al.* [38] and Zoundi *et al.* [21] also found similar results by analyzing TEC values of Surat and Niamey stations respectively.

The troughs observed at dawn reflect a decrease in photoionization at night and an increase in recombination events for both the FE and QA [39] [40]. The abrupt increase in TEC observed at sunrise is related to extreme ultraviolet radiation (EUV) and $E \times B$ upward vertical drift [41] [42]. According to Krishnank *et al.* [43], this increase is attributed to southerly winds.

3) Peaks are observed around 1400 TL during all solar phases. Concerning seasons, peaks are observed around 1500 LT during all seasons, but for winter season they are observed around 1400 LT. Peaks observed for FE's curves are

more significant than those of QA's curves, except during maximum phase and spring months. Peaks represent the greatest ionization during the day [21] [38].

4) The strongest positive storms are observed during the solar minimum phase and during the winter and fall months. Analyzing foF2 data variations at Dakar station, Sandwidi and Ouattara [44] observed similar results by showing that the weakest storms are observed during the increasing and decreasing phases and in summer months. FE predominate in the increasing and decreasing phases and in spring. This suggests that the strength of positive storms due to FE is not related to the occurrence of FE days.

5) Concerning, negative storms, the most intense are observed during maximum solar phase and spring season and the weakest during minimum solar phase (0300 LT and 0700 LT) and summer season (0300 LT and 2300 LT). Sandwidi and Ouattara [44] also found that the most negative storms are observed during maximum solar phase and spring months. It's also observed that FE are predominant in maximum than in minimum phase; and at spring than in fall. This suggests that on solar phases and seasonal scale, the strength of FE's negative storms is related to the occurrence of FE's days.

6) Most of negative storms are observed at night (0000 LT - 0200 LT) when chemical recombination is predominant, except in spring when they are recorded during all the day time. According to Fuller-Rowell *et al.* [13] negative storms result from variations in thermosphere composition during magnetic storms. Thus, an acceleration of the recombination process (with an increase in the N_2/O ratio) can be observed at solar maximum (~0000 LT and ~0400 LT), in spring (~0000 LT to ~0600 LT), and in summer (0000 - 0400 LT and 2100 LT to 2300 LT) during FE. This shows that losses due to chemical recombination exceed the plasma accumulation due to mechanical effects of the TNWC [45].

4. Conclusion

The study of TEC variations during FE over solar cycle 24 at Koudougou station showed that FE impact TEC variations during all solar phases and during all seasons. Storm strength analysis highlights that FE cause positive and negative storms on solar phases and seasons scales. FE's impacts are predominant during all solar phases, except maximum phase. Seasonal analysis also shows that FE's impact on TEC variations is important in all seasons, except in spring. Troughs observed at dawn reflect a decrease in photoionization at night and an increase in recombination phenomena. Negative storms are mostly observed in spring and a few times in summer and during maximum phase.

Data Availability

The sunspot data used to support the findings of our study are available at: https://www.sidc.be/silso/datafiles. The geomagnetic aa index data are available at https://isgi.unistra.fr/data_download.php.

Acknowledgements

The authors thank Rolland Fleury from IMT Bretagne, Technopole, Brest Iroise, France for his cooperation by providing Koudougou TEC data.

Conflicts of Interest

The authors declare no conflicts of interest regarding the publication of this paper.

References

[1] Kersley, L., *et al.* (2004) Total Electron Content—A Key Parameter in Propagation: Measurement and Use in Ionospheric Imaging. *Annals of Geophysics*, **47**, 1067-1091.

[2] Boutiouta, S. and Belbachir, A.H. (2006) Magnetic Storms Effects on the Ionosphere TEC through GPS Data. *Information Technology Journal*, **5**, 908-915. https://doi.org/10.3923/itj.2006.908.915

[3] Simon, P.A. and Legrand, J.-P. (1986) Some Solar Cycle Phenomena Related to the Geomagnetic Activity from 1868 to 1980. II. High Velocity Wind Streams and Cyclical Behavior of Poloidal Field. *Astron*omy and *Astrophysics*, **155**, 227-236.

[4] Chu, W., Ghahramani, Z. and Williams, C.K. (2005) Gaussian Processes for Ordinal Regression. *Journal of Machine Learning Research*, **6**, 1019-1041. https://www.jmlr.org/papers/volume6/chu05a/chu05a.pdf

[5] Nogueira, L., *et al.* (2011) Epicatechin Enhances Fatigue Resistance and Oxidative Capacity in Mouse Muscle. *The Journal of Physiology*, **589**, 4616-4631. https://doi.org/10.1113/jphysiol.2011.209924

[6] Astafyeva, E., Zakharenkova, I. and Doornbos, E. (2015) Opposite Hemispheric Asymmetries during the Ionospheric Storm of 29-31 August 2004. *Journal of Geophysical Research*: *Space Physics*, **120**, 697-714. https://doi.org/10.1002/2014JA020710

[7] Kelley, M.C. (2009) The Earth's Ionosphere: Plasma Physics and Electrodynamics. Academic Press, Cambridge.

[8] Picanço, G.A.S., *et al.* (2022) Study of the Equatorial and Low-Latitude Total Electron Content Response to Plasma Bubbles during the Solar Cycle 24-25 over the Brazilian Region Using a Disturbance Ionosphere index. *Annales Geophysicae*, **40**, 503-517. https://doi.org/10.5194/angeo-40-503-2022

[9] Baker, W.G. and Martyn, D.F. (1953) Electric Currents in the Ionosphere—The Conductivity. *Philosophical Transactions of the Royal Society of London. Series A, Mathematical and Physical Sciences*, **246**, 281-294. https://doi.org/10.1098/rsta.1953.0016

[10] Chapman, S. (1951) The Equatorial Electrojet as Detected from the Abnormal Electric Current Distribution above Huancayo, Peru, and Elsewhere. *Archives for Meteorology Geophysics and Bioclimatology, Series A*, **4**, 368-390. https://doi.org/10.1007/BF02246814

[11] Cowling, T.G. (1933) The Magnetic Field of Sunspots. *Monthly Notices of the Royal Astronomical Society*, **94**, 39-48. https://doi.org/10.1093/mnras/94.1.39

[12] Blanc, M. and Richmond, A.D. (1980) The Ionospheric Disturbance Dynamo. *Journal of Geophysical Research*: *Space Physics*, **85**, 1669-1686. https://doi.org/10.1029/JA085iA04p01669

[13] Fuller-Rowell, T.J., Codrescu, M.V., Moffett, R.J. and Quegan, S. (1994) Response of the Thermosphere and Ionosphere to Geomagnetic Storms. *Journal of Geophysical Research: Space Physics*, **99**, 3893-3914. https://doi.org/10.1029/93JA02015

[14] Matsushita, S. (1959) On Artificial Geomagnetic and Ionospheric Storms Associated with High-Altitude Explosions. *Journal of Geophysical Research* (1896-1977), **64**, 1149-1161. https://doi.org/10.1029/JZ064i009p01149

[15] Richmond, A.D., Matsushita, S. and Tarpley, J.D. (1976) On the Production Mechanism of Electric Currents and Fields in the Ionosphere. *Journal of Geophysical Research* (1896-1977), **81**, 547-555. https://doi.org/10.1029/JA081i004p00547

[16] Farley, D.T., Bonelli, E., Fejer, B.G. and Larsen, M.F. (1986) The Prereversal Enhancement of the Zonal Electric Field in the Equatorial Ionosphere. *Journal of Geophysical Research: Space Physics*, **91**, 13723-13728. https://doi.org/10.1029/JA091iA12p13723

[17] Akhoondzadeh, M. (2013) Support Vector Machines for TEC Seismo-Ionospheric Anomalies Detection. *Annales Geophysicae*, **31**, 173-186. https://doi.org/10.5194/angeo-31-173-2013

[18] Bolzan, M., Tardelli, A., Pillat, V., Fagundes, P. and Rosa, R. (2013) Multifractal Analysis of Vertical Total Electron Content (VTEC) at Equatorial Region and Low Latitude, during Low Solar Activity. *Annales Geophysicae*, **31**, 127-133. https://doi.org/10.5194/angeo-31-127-2013

[19] Ouattara, F., Zoundi, C., Amory-Mazaudier, C., Fleury, R. and Duchesne, P.L. (2011) Détermination du contenu électronique total à partir des pseudo distances (Pd) ou pseudo range (Pr) a la station de Koudougou au Burkina Faso. *Journal des Sciences*, **11**, 12-19.

[20] Verkhoglyadova, O.P., Tsurutani, B.T., Mannucci, A.J., Mlynczak, M.G., Hunt, L.A. and Paxton, L.J. (2014) Ionospheric TEC, Thermospheric Cooling and $\Sigma[O/N_2]$ Compositional Changes during the 6-17 March 2012 Magnetic Storm Interval (CAWSES II). *Journal of Atmospheric and Solar-Terrestrial Physics*, **115**, 41-51. https://doi.org/10.1016/j.jastp.2013.11.009

[21] Zoundi, C., Bazi, N., Kaboré, M. and Ouattara, F. (2021) Total Electron Content (TEC) Seasonal Variability under Fluctuating Activity, from 2000 to 2002, at Niamey Station. *International Journal of Physical Sciences*, **16**, 138-145. https://doi.org/10.5897/IJPS2021.4960

[22] Taoufiq, J., Mourad, B., Rachid, A. and Amory-Mazaudier, C. (2018) Study of Ionospheric Variability Using GNSS Observations. *Positioning*, **9**, 79-96. https://doi.org/10.4236/pos.2018.94006

[23] Mayaud, P.N. (1973) A Hundred Year Series of Geomagnetic Data, 1868-1967: Indices aa: Storm Sudden Commencements. *IAGA Bulletin No.* 33, IUGG Publications Office, Paris, 252 p.

[24] Ouattara, F., Amory-Mazaudier, C., Fleury, R., Duchesne, P.L., Vila, P. and Petitdidier, M. (2009) West African Equatorial Ionospheric Parameters Climatology Based on Ouagadougou Ionosonde Station Data from June 1966 to February 1998. *Annales Geophysicae*, **27**, 2503-2514. https://doi.org/10.5194/angeo-27-2503-2009

[25] Mayaud, P. (1971) Une mesure planétaire d'activité magnétique basée sur deux observatoires antipodaux. *Annales Geophysicae*, **27**, 67-70.

[26] Legrand, J.-P. and Simon, P.A. (1989) Solar Cycle and Geomagnetic Activity: A Review for Geophysicists. Part 1. The Contributions to Geomagnetic Activity of Shock Waves and of the Solar Wind. *Annales Geophysicae*, **7**, 565-593. https://ui.adsabs.harvard.edu/abs/1989AnGeo...7..565L

[27] Richardson, I.G., Cane, H.V. and Cliver, E.W. (2002) Sources of Geomagnetic Activity during Nearly Three Solar Cycles (1972-2000). *Journal of Geophysical Research*: *Space Physics*, **107**, Article No. 1187. https://doi.org/10.1029/2001JA000504

[28] Richardson, I.G., Cliver, E.W. and Cane, H.V. (2000) Sources of Geomagnetic Activity over the Solar Cycle: Relative Importance of Coronal Mass Ejections, High-Speed Streams, and Slow Solar Wind. *Journal of Geophysical Research*: *Space Physics*, **105**, 18203-18213. https://doi.org/10.1029/1999JA000400

[29] Ouattara, F. and Amory-Mazaudier, C. (2009) Solar-Geomagnetic Activity and Aa Indices toward a Standard Classification. *Journal of Atmospheric and Solar-Terrestrial Physics*, **71**, 1736-1748. https://doi.org/10.1016/j.jastp.2008.05.001

[30] Zerbo, J.-L, Amory Mazaudier, C., Ouattara, F. and Richardson, J. (2012) Solar Wind and Geomagnetism: Toward a Standard Classification of Geomagnetic Activity from 1868 to 2009. *Annales Geophysicae*, **30**, 421-426. https://doi.org/10.5194/angeo-30-421-2012

[31] Simon, P.A. And Legrand, J.-P. (1989) Solar Cycle and Geomagnetic Activity: A Review for Geophysicists. Part II. The Solar Sources of Geomagnetic Activity and Their Links with Susnspot Cycle Activity. *Annales Geophysicae*, **7**, 579-594

[32] Ouattara, F. and Amory-Mazaudier, C. (2012) Statistical Study of the Equatorial F2 Layer Critical Frequency at Ouagadougou during Solar Cycles 20, 21 and 22, Using Legrand and Simon's Classification of Geomagnetic Activity. *Journal of Space Weather and Space Climate*, **2**, Article No. A19. https://doi.org/10.1051/swsc/2012019

[33] Huang, N.-Y. and Cheng, K. (1996) Solar Cycle Variations of the Equatorial Ionospheric Anomaly in Total Electron Content in the Asian Region. *Journal of Geophysical Research*: *Space Physics*, **101**, 24513-24520. https://doi.org/10.1029/96JA01297

[34] Zou, L., *et al.* (2000) Annual and Semiannual Variations in the Ionospheric F2-Layer: I. Modelling. *Annales Geophysicae*, **18**, 927-944. https://doi.org/10.1007/s00585-000-0927-8

[35] Rishbeth, H., *et al.* (2000) Annual and Semiannual Variations in the Ionospheric F2-Layer: II. Physical Discussion. *Annales Geophysicae*, **18**, 945-956. https://doi.org/10.1007/s00585-000-0945-6

[36] Araujo-Pradere, E.A., Redmon, R., Fedrizzi, M., Viereck, R. and Fuller-Rowell, T.J. (2011) Some Characteristics of the Ionospheric Behavior during the Solar Cycle 23-24 Minimum. *Solar Physics*, **274**, 439-456. https://doi.org/10.1007/s11207-011-9728-3

[37] Vijaya Lekshmi, D., Balan, N., Tulasi Ram, S. and Liu, J.Y. (2011) Statistics of Geomagnetic Storms and Ionospheric Storms at Low and Mid Latitudes in Two Solar Cycles. *Journal of Geophysical Research*: *Space Physics*, **116**, Article No. A11328. https://doi.org/10.1029/2011JA017042

[38] Patel, N.C., Karia, S.P. and Pathak, K.N. (2017) GPS-TEC Variation during Low to High Solar Activity Period (2010-2014) under the Northern Crest of Indian Equatorial Ionization Anomaly Region. *Positioning*, **8**, 13-35. https://doi.org/10.4236/pos.2017.82002

[39] Warnant, R. (1996) Etude du comportement du Contenu Electronique Total et de ses irrégularités dans une station de latitude moyenne. Application aux calculs de positions relatives par le GPS. Université Catholique de Louvain, Ottignies-Louvain-la-Neuve. https://hdl.handle.net/2268/84721

[40] Sammuneh, M.A. (2003) Contribution au positionnement en temps réel par GPS: Prédiction de la correction ionosphérique. Ecole Doctorale Astronomie & Astrophysique d'Ile de France, Paris.

[41] Dabas, R., Singh, L., Lakshmi, D., Subramanyam, P., Chopra, P. and Garg, S. (2003) Evolution and Dynamics of Equatorial Plasma Bubbles: Relationships to ExB Drift, Postsunset Total Electron Content Enhancements, and Equatorial Electrojet Strength. *Radio Science*, **38**, Article No. 1075. https://doi.org/10.1029/2001RS002586

[42] Hajra, S., Maity, S. and Roy, S. (2016) Regioselective Friedel-Crafts Reaction of Electron-Rich Benzenoid Arenes and Spiroepoxyoxindole at the Spiro-Centre: Efficient Synthesis of Benzofuroindolines and 2*H*-Spiro[benzofuran]-3, 3'-Oxindoles. *Advanced Synthesis & Catalysis*, **358**, 2300-2306. https://doi.org/10.1002/adsc.201600312

[43] Krishnank, K.A., Mahadevan, H., Aswathy, H., Suranya, K., Dev, V.V. and Antony, S. (2019) Geochemical Aspects of Estuarine System in the Cochin Port Trust Area: Appraisal of Adsorption Properties of Pb (II), (Cd II), Zn (II) and Cu (II) onto the Sediment Clay Fraction. *Journal of Applied Geochemistry*, **21**, 398-403. https://search.proquest.com/openview/d62bcaceac2bd28d6effb9adecbacafd/1?pq-origsite=gscholar&cbl=2029688

[44] Sandwidi, S.A. and Ouattara, F. (2022) Recurrent Events' Impacts on foF2 Diurnal Variations at Dakar Station during Solar Cycles 21-22. *International Journal of Geophysics*, **2022**, Article ID: 4883155. https://doi.org/10.1155/2022/4883155

[45] Balan, N., Souza, J. and Bailey, G.J. (2018) Recent Developments in the Understanding of Equatorial Ionization Anomaly: A Review. *Journal of Atmospheric and Solar-Terrestrial Physics,* **171**, 3-11. https://doi.org/10.1016/j.jastp.2017.06.020